Environmental Fluid Mechanics (2025) 25:25
https://doi.org/10.1007/s10652-025-10036-2

ORIGINAL ARTICLE

Laboratory experiments on Dense Shelf Water formation

Nathan Cadot[1,2] · Carlo Camporeale[1] · Luca Ridolfi[1] · Pietro Salizzoni[1,2]

Received: 3 December 2024 / Accepted: 1 April 2025

Abstract

Polynyas—ice-free regions within sea ice—play a critical role in the sea ice production and the formation of Dense Shelf Water (DSW) in Antarctica. This dense water, formed as salt is expelled from freezing saline water (the so-called brine rejection), descends the continental slope, contributing to the formation of Antarctic Bottom Water, a key component of global thermohaline circulation. Despite the significance of polynyas and their influence on climate regulation, clear experimental evidence that brine rejection alone is capable of inducing DSW currents is lacking. This study aims to fill that gap by conducting controlled laboratory experiments simulating polynya-like conditions. Using particle image velocimetry, the velocity field in a water tank was measured under conditions of brine rejection. Experiments show that brine rejection does indeed induce gravity currents. Their flow rate was found to be dependent on the opening size of the polynya and on the geometry of the slope on which the current flows. These preliminary experiments offer a new experimental framework for studying gravity currents driven by brine rejection.

Highlights

- A novel laboratory setup to simulate gravity flows induced by brine rejection.
- The first laboratory-scale study of Dense Shelf Water formation due to polynya-likedynamics.
- We show that localized brine rejection initiates density-driven flows with a velocityof the order of magnitude of millimeters per second.

✉ Nathan Cadot
nathan.cadot@polito.it

Carlo Camporeale
carlo.camporeale@polito.it

Luca Ridolfi
luca.ridolfi@polito.it

Pietro Salizzoni
pietro.salizzoni@ec-lyon.fr

[1] Department of Environment, Land, and Infrastructure Engineering, Politecnico di Torino, Corso Duca degli Abruzzi 24, 10129 Turin, Italy

[2] Laboratoire de Mécanique des Fluides et d'Acoustique, Ecole Centrale de Lyon, 34, Avenue Guy de Collongue, 69134 Ecully, France

Published online: 25 April 2025

Keywords Polynya · Brine rejection · Gravity currents · Dense Shelf Water

1 Introduction

Polynyas are ice-free regions within sea ice that persist throughout the winter, typically formed by either upwelling of warm water (sensible heat polynyas) or mechanical forcing (latent heat polynyas) [31]. Mechanical forcing is generally attributed to currents or wind, notably katabatic winds, which are the primary drivers of important polynyas in coastal areas of Antarctica [7]. The Antarctic latent heat polynyas are often referred to as 'ice factories' due to their substantial production of frazil ice. Although they represent only about 1% of the total sea ice extent, they account for up to 10% of the total sea ice volume production in the Southern Ocean [26].

The formation of sea ice from saline water triggers a process known as brine rejection, where large amounts of salt are expelled back into the ocean [11]. As a result, salt accumulates in the waters of Antarctic latent heat polynyas, which are typically located over the continental shelf. This process leads to the formation of Dense Shelf Waters (DSW) [23]. Another significant source of DSW, often working in tandem with brine rejection, is the input of supercooled water from ice-ocean interactions at the base of floating ice shelves [9].

DSW can descend the continental slope and contribute to the formation of Antarctic Bottom Water (AABW), which is a key driver of the global thermohaline circulation, an essential component of Earth's climate regulation system [12]. Despite the importance of AABW, the specific conditions leading to its formation are still not fully understood. It is clear that there is a need for a significant increase in the density of surface water so that it can flow down the continental slope. The density of AABW is very high with respect to surface water because it is colder and more saline. It is generally hypothesized that the continental shelf beneath polynyas facilitates the accumulation of density coming from the brine rejection by reducing the mixing with the surrounding water and allowing shelf waters to get dense enough to flow down the slope and form AABW. However, the necessary size of the plateau for such accumulation is not well-defined [3]. Indeed, some polynyas do not produce DSW and some polynya induce AABW formation even without a large continental shelf (for example the Cape Darnley polynya) [22]. The factors affecting the production of brine rejection in polynyas and their temporal evolution are not fully understood, especially the impact of seasonal and meteorological forcing [24].

Furthermore, the dynamics of DSW cascading down the continental slope are poorly described due to the challenges associated with obtaining underwater measurements in these remote regions. Submarine canyons along the slope have been suggested to play a role in directing these flows [2]. However, many small-scale and local processes affecting DSW formation and its downslope flow remain poorly understood. These include tidal influences on the continental shelf, the influence of the topography of the bottom, the entrainment of seawater, the mixing of the DSW with other water masses, turbulence-induced processes, the role of shelf meltwater, and the interaction of brine plume with water stratification [24]. This lack of understanding leads to uncertainties in the numerical models used for climate simulations [13].

Given the challenges inherent in conducting field measurements about DSW and AABW, one might expect experimental studies to be prevalent. Such studies offer the advantage of controlled environments, allowing for precise measurements of different

variables. However, experimental studies in this area remain scarce. The closest attempt at replicating a polynya in the laboratory was conducted by Ushio and Wakatsuchi in [28], where an air flow was applied over a water tank in a cold room to simulate polynya conditions. The limited number of laboratory studies is likely due to the substantial challenges inherent in reproducing such complex phenomena within controlled settings.

The cascading of DSW down the continental slope is analogous to gravity currents, namely flows driven by buoyancy differences. In the context of AABW formation, the increase in density arises from higher salinity and lower temperatures. Gravity currents have been extensively studied, in particular, many experimental studies have been carried out with an influx of saline water as a source of buoyancy [5, 19, 29]. Sinking gravity currents along slopes, with or without stratification, are a common focus of these studies [18]. Various sources of buoyancy for gravity currents and plumes have been studied. Mainly, heat flux, influx of saline water, or gases heavier than air (CO_2 for example) were considered as triggers of density gradients [21].

The generation of buoyancy in the case of a polynya, other than the sea-surface cooling due to exchanges with the colder atmosphere, is the brine rejection. The brine rejection is the expulsion of the salt from the crystalline structure when ice forms from salty water. Its phase change is peculiar and different from the simple addition of saline water or the heating of a surface without phase change. Even though several authors noted the clear similarities between DSW flowing down the continental slope and gravity currents, no published article presented experiments using brine rejection as a source of buoyancy to induce gravity current. These authors worked mainly with numerical simulations or experiments involving the addition of saline water [4, 10].

Although not investigated as a buoyancy source, many aspects of brine rejection have been studied, both with laboratory experiments [20] and numerical simulations [17]. The study that proposed experiments closest to using brine rejection as triggers of density gradients was [8]. In this article the convection induced by brine rejection in a tank of water was studied; the brine rejection was homogeneous at the surface of the water and not confined in a polynya.

In this general picture, two key open questions are addressed in this study: is brine rejection alone capable of generating a gravity current? If so, how does the latter depend on the system geometry (i.e., spatial extent of brine rejection and topography of the bottom)?

This study aims to shed light on the above questions by conducting a preliminary laboratory study, in which polynya-like conditions are reproduced. The focus is on the effects of brine rejection on the velocity field within a water tank. The experiments were conducted in a cold room where ice was allowed to form on part of the water surface, creating conditions similar to a polynya. To assess the influence of brine rejection, the experiments were performed using both saline and freshwater, and the velocity field was measured using particle image velocimetry (PIV).

This preliminary study aims to provide novel laboratory data on polynyas, filling a gap where previous analog studies are lacking.

2 Experimental setup and methodology

2.1 Setup

The experiments were carried out in the Water Engineering Laboratory of the Department of Environment, Land and Infrastructure Engineering (DIATI) of the Politecnico di Torino in Italy. The schematics and pictures of the experimental setup are shown in Fig. 1. It consists of a tank made of stainless steel for the structure and glass for the walls sizes of 1.5 m × 0.70 m × 0.55 m, filled with fresh or salt water (Fig. 1a, b). The axis system is $\{x,z\}$, with x being the horizontal axis and z the vertical (see Fig. 1a). The point (0,0) is located in the upper-right angle of the water body and both axes are directed toward the tank (the x-axis is directed toward the left and the z-axis is directed toward the bottom). The tank was placed inside a cold room maintained in a temperature range of − 5 to − 20 °C, with a precision of ±1 °C. The temperature within the cold room is homogenized by fans, ensuring a consistent thermal distribution around the target temperature. The system operates by allowing the temperature to decrease by one degree below the target before deactivating the cooling mechanism. Once the temperature increases to one degree above the target, the cooling system is reactivated, thereby maintaining the desired thermal conditions. To insulate the tank from external temperature, the walls were surrounded by a 20 cm thick layer of polystyrene. Two geometries were considered one with a vertical wall and one with a 45° inclined wall starting at the free surface. To simulate a polynya, most of the free surface was covered with a 20 cm thick layer of polystyrene, mimicking the insulation provided by a thick ice pack. An area of open water was preserved at one end of the tank. Its width was equal to the tank width and three different lengths, L, (see Fig. 1b) were used during the experiments: 25 cm, 35 cm, 45 cm. Two different kinds of experiments were carried out: an experiment which aimed at measuring the velocity field inside the tank and an experiment which aimed at measuring the salt flux generated by the brine rejection.

An insulated box was constructed within the cold room to house the instrumentation (Fig. 1c, d). This insulated box was maintained at a temperature of approximately −1°C using a heating system. This setup ensured that the glass wall inside the box maintained no flux conditions, with the water temperature during the experiments being around −1.2°C.

Velocity measurements were obtained using the particle image velocimetry (PIV) technique. A laser plane was created in the x-z plane by two lasers MDL-III 520 nm, 300 W, 30° angle from CNI Laser positioned beneath the tank. A Nikon Z5 camera, housed inside the insulated box, recorded the water movements at 24 frames per second. The PIV method used was a simplified version. Due to the slow movement of the water in these experiments (of the order of magnitude of the millimeter per second), a constant laser sheet was sufficient, and the natural impurities in the water served as tracers. The recorded videos were processed using the PIVlab software from Matlab to determine the velocity fields [27]. One image out of every two from the video was used, resulting in a relative acquisition sampling frequency of 12 Hz. Interrogation windows were chosen to be 128×128 pixels^2 with an overlap of 50 %. This allowed us to obtain one vector for every centimeter. The measurement area was 33 cm × 59 cm and was situated 13 cm deeper than the free surface and 5 cm above the bottom.

Salinity measurements were obtained using an OAKTON 35419-35 CON 550 Series Benchtop Conductivity Meter Kit. This instrument allows for a precision of 0.1 g/L. The

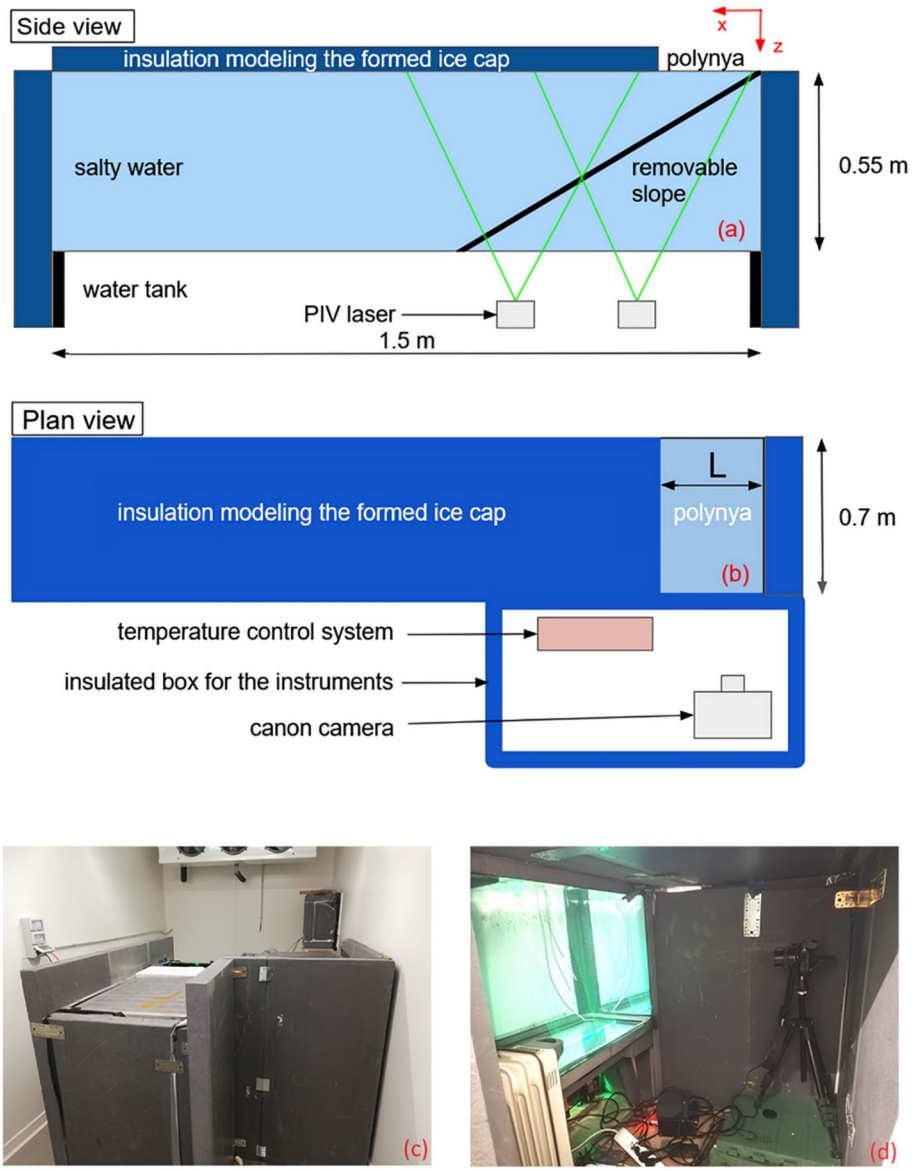

Fig. 1 Schematics **a**, **b** and pictures **c**, **d** of the experimental setup: **a** side view, **b** top view, **c** experimental setup in the cold room, **d** inside of the insulated box with the PIV system

salinity measurements were used for the setup of the experiments, as well as to measure the salt flux released by the brine rejection.

Furthermore, four PT100 temperature measurement probes, with a precision of $\pm 0.2°C$, were immersed in water along the wall at four different depths (respectively 5 cm, 19.5 cm, 34 cm, and 38.5 cm below the surface of the water). The probes were connected to a Data Acquisition System (DAQ) from National Instruments to monitor the temperature of

the water. A calibration of five points (− 5 °C, − 2 °C, 0 °C, 2 °C, 5 °C) was performed before taking the measurements. The temperature measurement allowed us to control the experimental conditions with regard to the water temperature. The temperature of the water in the tank was −1.2 °C for the salinity 34 PSU and −2.6 °C for the salinity 70 PSU with a precision of 10% (notice that these temperatures are close to the corresponding freezing point of the salty water). The water was stirred to ensure homogeneity of the temperature.

2.2 Runs

The experiments aimed to investigate the effect of brine rejection in polynya-like conditions. To do this, the velocity field in the tank and the salt flux released by the brine rejection were measured.

The experimental procedure was as follows:

1. the cold room temperature was adjusted to the desired setting, which typically requires a few hours to stabilize;
2. the water was cooled to its freezing point as a result of thermal exchanges with the cold air. Usually, it takes twelve hours depending on the initial temperature of the water so it was initiated the day before the experiment;
3. when the temperature of the water was close to its freezing point (which depends on the salinity [6]) the water was stirred with a stick to ensure homogeneity;
4. the water was allowed to settle for five minutes to wait for the dissipation of the movements in the water and the formation of the ice;
5. when the ice started forming at the surface of the polynya, the PIV measurement was set for 30 min;
6. 30 min after the ice started to form on the polynya surface, the PIV measurement was stopped, and then the ice was retrieved with a net;
7. the retrieved ice was melted, and its salinity and volume were measured. The salinity in the melted ice and in the salt water were compared, and the salt flux was computed according to the relation $(S_{water} - S_{ice}) \cdot V_{ice}/(A \cdot T)$, where S_{water} is the salinity of the water, S_{ice} and V_{ice} are the salinity and the volume of the melted ice, respectively, A is the area of the open free-surface and T is the duration of the experiment.

This experimental procedure was chosen after trying various methods to keep a polynya open. The original aim was to use an air flow to open and sustain the artificial polynya. This procedure, described by Ushio and Wakatsuchi [28], involved using airflow over the aquarium in the cold room to create and maintain a polynya. The study demonstrated that the polynya gradually closes over time. The same procedure was applied here: a fan and a convergent nozzle were used to induce an air flow at the water surface. This enabled the polynya to remain open for a brief period. However, the air flow induced excessive movement in the water, generating surface waves and internal fluid cells, due to wind shear stresses. This interference masked the actual effect of brine rejection while being insufficient to maintain an open polynya for an extended period. Therefore, a simpler procedure was adopted. The absence of wind introduces a difference in the type of ice formed compared to that in a natural polynya. In polynyas, frazil ice (i.e., a collection of randomly oriented ice crystals) is typically produced, whereas without wind a more coherent, mushy layer of consolidated ice forms. Both differ from the solid slab of ice commonly observed in freshwater. Brine rejection occurs in both types of ice but in a different way. In frazil ice,

almost all the salt is rejected at the formation of the ice crystals, whereas in consolidated ice, a part of the salt is rejected in the surrounding water, and a part is trapped inside the ice in the form of brine cells. The brine is then slowly released via drainage channels. For the experiment we are presenting the practical difference is that the consolidated ice will reject less brine than frazil ice.

During the experimental campaign, various conditions were tested to investigate the effects of different parameters (Table 1 is a summary of these conditions). Two temperatures (− 10 °C and −20°C) were chosen, both within the cold room's operational range (the cold room temperature of −5°C was not selected because ice formation was too slow at this temperature). Three salinities (0 PSU, 34 PSU, and 70 PSU) were used: 0 PSU is fresh water, i.e. the benchmark test, 34 PSU represents typical Antarctic Ocean salinity [25], while 70 PSU, being double, was used to assess the influence of salinity on brine rejection. Three different opening sizes L of the polynya (25 cm, 35 cm, and 45 cm) were tested to determine if a wider opening would amplify the effect of brine rejection. Lastly, two geometries (vertical wall and 45° inclined wall) were examined to compare the flow behavior on a slope versus a vertical surface. The different combinations of the parameters give 24 cases with salt and two cases without salt (i.e. a total of 26 different cases). For the control tests without salt, only the geometry was changed, the air temperature was set to −20°C, and the opening size to 35 cm. For each combination of the parameters, the experiment was repeated at least twice to ensure repeatability, obtaining a total of 83 experiments with salt and 10 experiments without salt.

2.3 Pre-processing of the measures

In the 83 experiments conducted with salt water, the water in the tank exhibited some kinematic patterns resembling gravity currents or convective cells. These patterns will be presented in detail in the Result section.

Note that the duration of ice formation and brine release is significantly longer than the 30-min interval during which we acquire velocity measurements. We can therefore consider that this experimental window allows us to observe the velocity field in a (statistically) quasi steady-state.

Among these saline experiments, some were found to be fairly steady (albeit with fluctuations) during the 30 min of the recording, while others showed clear trends; namely, the velocity field and flow rate of the brine-induced gravity current showed a significant temporal evolution and were not in a statistically steady state. It follows that a selection was necessary to identify the most reliable cases. The aim was in fact to obtain a pseudo-steady state (possibly after an initial period of flow pattern formation) that lasts for 30 min, in which it was then possible to average to eliminate short-term fluctuations.

Table 1 The different experimental conditions

Opening size L	25 cm	35 cm	45 cm
Temperature	− 10 °C	− 20 °C	
Salinity	0 PSU	34 PSU	70 PSU
Geometry	Vertical wall	45 degree inclined wall	

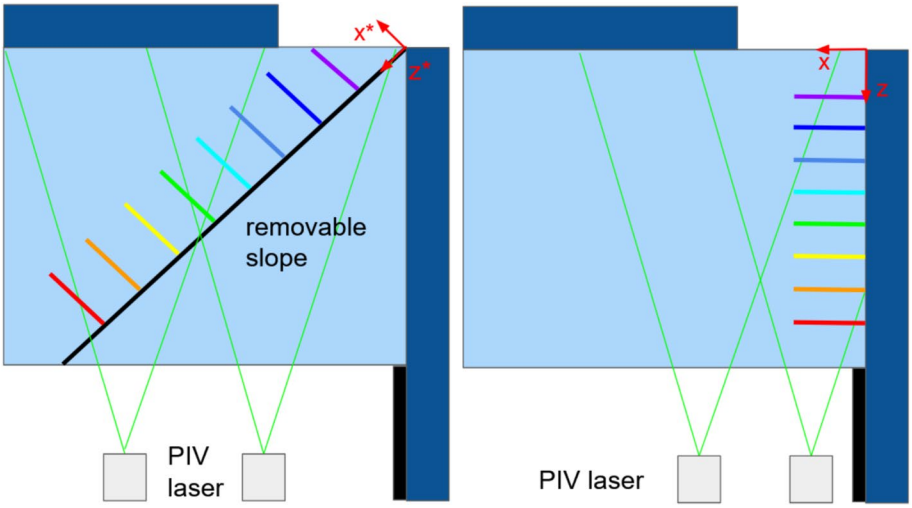

Fig. 2 Localization of the sections (perpendicular to the wall) where the velocity profiles were measured and flow rates were evaluated. The colors of the sections are the same as the colors of the velocity profiles reported in Fig. 6

To select the steady cases, the flow rate of the observed current was calculated at eight regularly spaced depths along the wall, using the vector field retrieved by PIVlab (see Fig. 2). To determine the flow rate at a specific point, the velocity was integrated along a line normal to the wall. The axis normal to the wall changes depending on the geometry of the experiment. For the case with a vertical wall, the axis normal to the wall is x and the axis parallel to the wall is z, while for the case with the inclined wall, the axis normal to the wall is x^* and the axis parallel to the wall is z^* (see Fig. 2). The integration was carried out over the distance from the wall to the location where the velocity component parallel to the wall (z or z^* depending on the geometry) becomes zero. This gives a result in cm^2/s which is a planar flow rate (the flow being considered planar as will be explained in more detail in the Result section). This calculation was performed for one frame every 10 frames, resulting in one value every 0.8 s. This generated a time series of flow rates at different transects along the slope, showing the flow evolution over time. Only experiments exhibiting simple oscillation patterns around a mean value, with no particular trend, were retained. The Student's t-test [1] was applied to the time series to test for the presence of a trend: when the p value was greater than 0.05, no significant statistical trend was assumed. Figure 3 shows one of these time series in which there are fluctuations around a stable mean value, and the trend is non-significant (p value = 0.8).

In this way, we eliminated runs where, due to the imperfect control of the experimental conditions, unsteady kinematic patterns were manifested.

A total of 32 cases successfully passed the stationarity test and were deemed valid for analysis. These included 19 cases with a vertical wall and 13 cases with an inclined wall.

Finally, it is worth noting that some cases were repeated in order to evaluate the reliability of the experiments. In particular, two cases—(i) temperature of − 20 °C, salinity of 34 PSU, an opening of 45 cm, inclined wall and (ii) temperature of − 20 °C, a salinity of 70

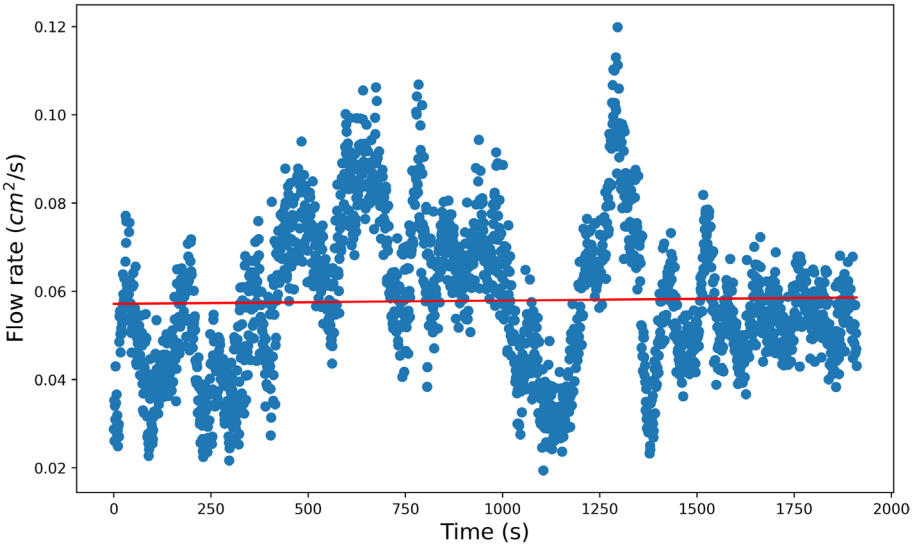

Fig. 3 Flow rate as a function of time in a transect located 30 cm beneath the surface of the water. In red the linear regression (p value=0.8, the trend is statistically non-significant). The experimental conditions were: − 20 ˚C for the cold room temperature, 35 cm for the polynya opening, an inclined wall of 45 degrees, and a salinity equal to 34 PSU

PSU, an opening of 35 cm, inclined wall—were repeated four times. In all repetitions, we found differences in the values of q and H less than 10%. This demonstrates that the experiments presented here exhibit a good level of repeatability.

3 Results

3.1 Flow fields

The role of brine rejection in generating buoyancy and inducing a gravity current was investigated. Figure 4 illustrates some exemplifying cases, where the effect of brine rejection on the velocity field is compared to corresponding control cases with freshwater, where brine rejection was absent. The experiments with freshwater were performed to check that the experimental system behaved as expected, that the measurements were correct, and to highlight the key changes due to the salt addition. There are two main differences between the case with the freshwater and that with the salt water. The first one is the dependence of the density on the temperature: for the freshwater, density exhibits a maximum at 4 °C which does not occur for salty water. In our experiments—as the formation of ice at the top of the domain establishes an upper boundary condition of 0 °C—the non-monotonic behavior of density leads to a stable stratification in the case of the freshwater. However, it should be noted that, in the experiments, the temperature of the water was nearly uniform and close to 0 °C, while the bottom of the tank was only about 0.3 °C warmer than the top (a difference close to the precision limit of the temperature

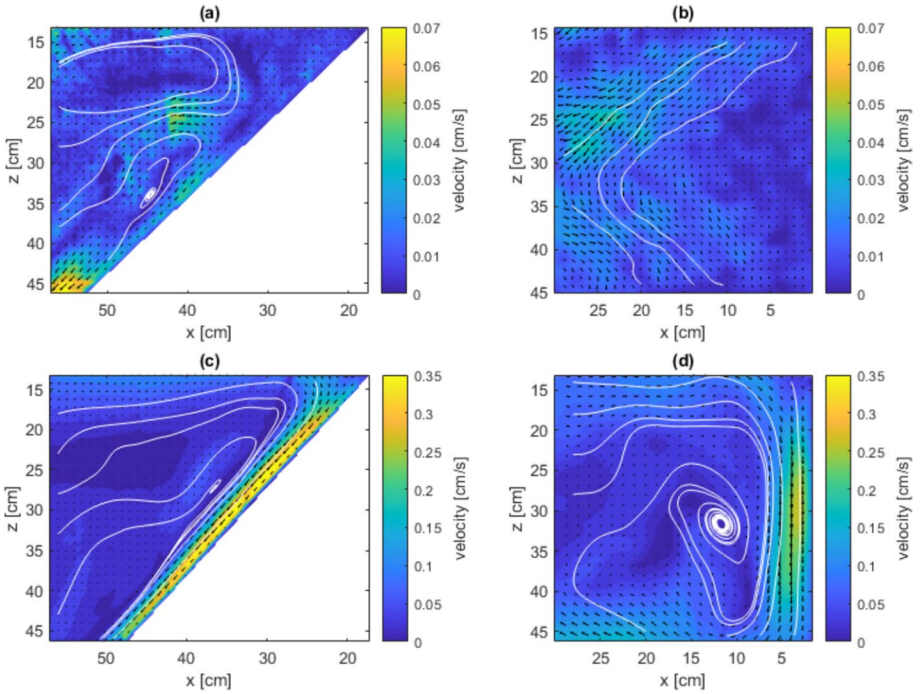

Fig. 4 Mean velocity field averaged over 30 min. The axes x and z are defined in Fig. 2. The cold room was set to − 20 ◦C and the polynya had an opening size of 35 cm in all four cases (i.e., from $x = 0$ to $x =$ 35 cm). Panels (**a** and **b**) refer to fresh water, while panels (**c** and **d**) refer to salt water (34 PSU); left/right correspond to inclined/vertical walls respectively. It should be noted that the color scales for the fresh and salt water cases are different

measurement), indicating a minimal stratification. The second difference is the brine rejection, which doesn't occur in the freshwater case.

All the measurements presented here are planar, and evaluated on the vertical measurement plane located in the midpoint of the tank. Other parallel plans showed similar results. In fact, some measurements on a perpendicular plan were made to test the presence of 3D patterns, but no relevant 3D motions were detected. Thus, we consider that the flow is mainly two-dimensional and that the middle plan is representative of all other parallel planes.

Four cases are compared in Fig. 4: 45° inclined wall and fresh water (panel a), vertical wall and fresh water (panel b), 45° inclined wall and salt water (panel c), and 45° inclined wall and fresh water (panel d). In all cases, the cold room was set to a temperature of − 20 °C, and the polynya had an opening size of 35 cm (the free-surface opening extends from $x = 0$ to $x = 35$ cm, see Fig. 1). In Fig. 4, the location of the polynya-like opening is on $z = 0$ cm, above the image.

Figure 4 shows a marked difference between the experiments with and without salt. The experiments with salt water exhibit distinct gravity currents along the wall, whereas the experiments with fresh water show a (weak) cellular pattern (panels a) or incoherent movements (panels b). The magnitude of the velocity field also differs significantly between salt and fresh conditions. In the fresh water, the velocity magnitude

is of the order of 10^{-2} cm/s (0.025 cm/s for the vertical wall and 0.035 cm/s in the case of the inclined wall), while in the salt water condition, it is of the order of 10^{-1} cm/s (0.2 cm/s and 0.25 cm/s in the case of the vertical and the inclined wall, respectively). In the fresh water the small movements are quite randomly distributed, erratic, and are unable to create clear flow patterns. Additionally, we noted a considerable variability of the velocity field (particularly in the case of the vertical wall) between different realizations of the same experimental conditions; this demonstrates the lack of a clear pattern and the extreme sensitivity to small differences in initial or boundary conditions. Thus, in the absence of salt, the water is almost at rest, with very weak residual cellular or incoherent motions arising from the stirring of the water at the start of the experiment.

In contrast, when salt was present, the formation of a clear gravity current along the wall was observed, and velocities were an order of magnitude greater than in the freshwater case. This current was consistently observed across all experiments, with variations between experiments being much less pronounced than those in the fresh water condition. Therefore, the presence of salt in the water has a significant impact, which can be attributed to the brine rejection. The temperature measurements show a homogeneous temperature along the wall. This strengthens the relationship between observed currents and brine rejection to the exclusion of potential thermal effects. In polynyas, brine rejection acts as a source of buoyancy, increasing local salinity and, consequently, water density.

A notable difference between the experiments with a vertical wall and an inclined wall occurs (see Fig. 4 panels b and d): in the case of an inclined wall, the current develops over a greater length and becomes more pronounced and localized along the wall. This can be due to two effects: the first is linked to the greater length of the inclined wall (about 1.4 longer than the vertical one), and the second effect is the capability of the inclined wall to intercept the brine rejection over almost the entire length of the opening at $z = 0$ cm; differently, the vertical wall 'collects' the salt released by the freezing of the water in a smaller portion of the polynya-like opening.

3.2 Vorticity fields

To gain a clearer understanding of the general flow structure, it is insightful to analyze the vorticity fields presented in Fig. 5. Similar to the velocity fields, these plots reveal a stark contrast between the cases without salt water (Fig. 5a–c) and those with salt water (Fig. 5b–d). In the former, no distinct spatial patterns in the vorticity are observed, indicating the unstructured nature of the flow. Conversely, the saltwater cases display layers of vorticity with opposite signs emerging near the lateral walls, whether inclined or not.

Understanding these patterns requires recalling that vorticity arises from two primary mechanisms. The first is the diffusion of (positive) vorticity from the walls, driven by velocity gradients imposed by the no-slip boundary condition. The second is the generation of vorticity due to density gradients, also referred to as 'baroclinic generation of vorticity' [30], expressed as $\vec{S}_\rho \times \vec{g}$, where $\vec{S}_\rho = \nabla(\ln \rho)$ is the so-called stratification vector. Close to the solid boundary, the flow develops a thin layer of positive (i.e., counterclockwise) vorticity, highlighting the dominant role of positive velocity gradients imposed by the no-slip condition at the wall (Fig. 5). This thin layer is overlain by a

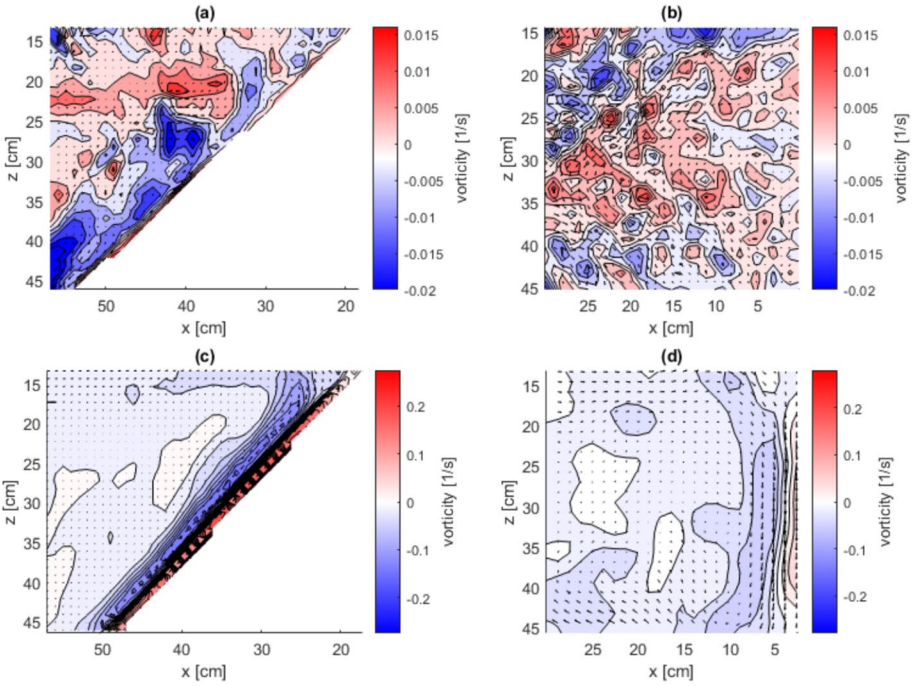

Fig. 5 The figure shows the same velocity fields as in Fig. 4, reporting the vorticity field in the background

thicker layer of negative vorticity due to the action of $\vec{S}_\rho$. This pattern therefore reflects the persistent presence of a denser fluid layer flowing along the lateral walls, driven by continuous brine rejection at the water surface.

The two saltwater cases also exhibit a background of negative vorticity, indicating the presence of a wall-structured, clockwise, large-scale recirculating motion induced by the sinking of the dense fluid layer.

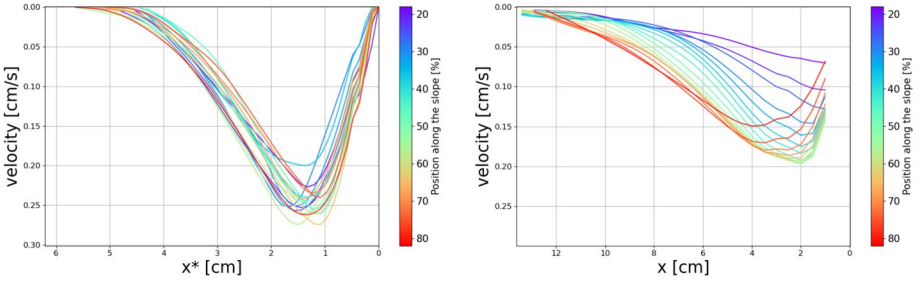

Fig. 6 Velocity profiles at different transects along the inclined (on the left) and the vertical (on the right) walls. The color represents the percentage of the wall length traveled by the current: 0% is the freezing free-surface and 100% is the bottom of the tank

3.3 Velocity profiles

To describe the kinematics of the gravity current along the wall, some velocity profiles were evaluated (see Fig. 6). The velocity profiles were located uniformly along the wall; their positions are shown in Fig. 2. The axis along which the velocity profiles are taken are x^* for the inclined wall and x for the vertical wall as defined in Fig. 2. The component of the velocity that is shown is parallel to the wall (i.e., along the z and z^* axis, respectively). Velocity profiles are obtained from the velocity field averaged over 30 min in the measurement window, the flow regions close to the surface and the bottom were not measured. In the case of the vertical wall, a zone of around 0.1 cm from the wall could not have been measured due to technical limitations in the PIVlab software. This explains why the velocity is not seen reaching zero at the wall when the wall is vertical; this limitation was not present in the inclined case, allowing for more accurate measurements near the wall. The profiles are shown from the wall to the point where the velocity reaches zero.

Two cases are presented: one refers to the vertical wall and one to the inclined wall. These two cases represent well what was observed in the other experiments. Both cases had identical experimental conditions, except for the wall geometry; specifically: the cold room temperature was − 20 °C, the salinity was 34 PSU, and the polynya opening size was 35 cm.

Vertical and inclined walls exhibit common features: they show comparable velocities (around 0.1−0.2 cm/s), profiles have similar shapes, and, starting from 60% along the vertical wall, profiles are quantitatively quite similar to those measured on the inclined wall. However, they also exhibit some key differences. The first notable difference is the thickness of the gravity current, that is the distance from the wall of the point where the velocity reaches zero. It is larger in the case of the vertical wall (about 12 cm) than in the case of the inclined wall (about 5 cm). This can again be attributed to geometric factors: the inclined wall facilitates the collection of descending motions (induced by brine rejection) that develop along the full length of the opening; leading to steeper density gradients in the gravity current, which becomes more 'concentrated ' into a reduced thickness. This greater 'salt collection' by the inclined wall also explains the higher velocity reached by the gravity current in the case of an inclined wall.

The second difference is the dependence of the velocity on depth. For the vertical wall, there is a clear progression: the velocity increases and then decreases with depth. The shape also develops from a flat profile to a bell-like profile. In contrast, for the inclined wall, the depth-wise evolution is less pronounced, and the profiles are more similar to each other. The difference between the two cases can be attributed to the different motion patterns: in the case of a vertical wall, a convective cell develops near the wall and we measured a vertical portion of it—therefore, velocity profiles are affected by the curvature of the trajectories in the initial and final measurement sections—instead, in the case of an inclined wall, a density current develops (on a path that is also longer than the vertical wall) which shows an almost self-similarity of the profiles.

The inclined wall case is thus more similar in shape to a classical gravity current, such as one formed by introducing a saline flow into the water, while the vertical wall case exhibits characteristics more akin to Rayleigh–Bénard cells [15]. In both cases, the descent of the denser water generates a large-scale recirculating motion; however, in the inclined wall case, the recirculating cell is more diffuse and less well-defined compared to the more prominent structure observed in the vertical wall case.

Table 2 Flow rate and flow thickness depending on the experimental parameters

	Vertical wall			Inclined wall (45°)		
q (10^{-1} cm^2/s)	25 cm	35 cm	45 cm	25 cm	35 cm	45 cm
34 PSU – 20 °C	20	9.2	13	5.7	6.2	7.7
70 PSU – 20 °C	11	11	14	4.5	8.2	8.7
34 PSU – 10 °C	6.1	11	No data[1]	13	11	13
70 PSU – 10 °C	4.7	14	22	1.7	2.4	3.4
	Vertical wall			Inclined wall (45°)		
H (cm)	25 cm	35 cm	45 cm	25 cm	35 cm	45 cm
34 PSU – 20 °C	12	12	18	5.1	5.0	6.5
70 PSU – 20 °C	7.4	7.6	11	4.1	5.2	5.3
34 PSU – 10 °C	7.4	8.9	No data[1]	9.3	6.9	6.7
70 PSU – 10 °C	5.8	16	22	3.4	4.6	7.0

[1] Data not available due to backup issues

3.4 Dependence on experimental parameters

The study investigated the influence of four parameters on the gravity current generated by brine rejection: salinity, external temperature, wall inclination, and opening size of the polynya. Table 2 illustrates the values of the flow rate (q) and the thickness of the gravity current (H). This latter is defined as the distance from the wall to the point where the z^* component of the velocity reaches zero. The flow rate per unit length (expressed in cm^2/s) is defined as $q = \int_0^H u(x^*)dx^*$, where $u(x^*)$ is the z^*-component of the velocity.

Salt flux measures are presented in Table 3. They were obtained at the end of the experiments by measuring the salinity and the volume of the ice (see Sect. 2.2). The ice was found to be 20% less salty than the seawater. Additionally, approximately four times more ice formed when the cold room temperature was − 20 °C compared to − 10 °C. As expected, measured data indicate that the salt flux increases with higher salinity and lower temperatures. Specifically, the salt flux approximately doubles when the salinity increases from 34 to 70 PSU and quadruples when the temperature decreases from − 10 °C to − 20 °C.

Table 2 shows a large variability for both q and H. The flow rate q goes from 0.17 cm^2/s in the case with $L = 25$ cm, 70 PSU salinity, − 10 °C air temperature, and inclined wall to 0.25 cm^2/s when $L = 45$ cm, 34 PSU, − 20 °C, and vertical wall. The current width H goes from 1.6 cm for $L = 35$ cm, 70 PSU, − 10 °C, and vertical wall to 18 cm for $L = 45$ cm, 34 PSU, − 20 °C, and vertical wall. Thus, there is one order of magnitude

Table 3 Brine-rejection-salt flux, depending on the water salinity and air temperature

Salt flux	− 10 °C	− 20 °C
34 PSU	0.003 g/m^2/s	0.01 g/m^2/s
70 PSU	0.005 g/m^2/s	0.02 g/m^2/s

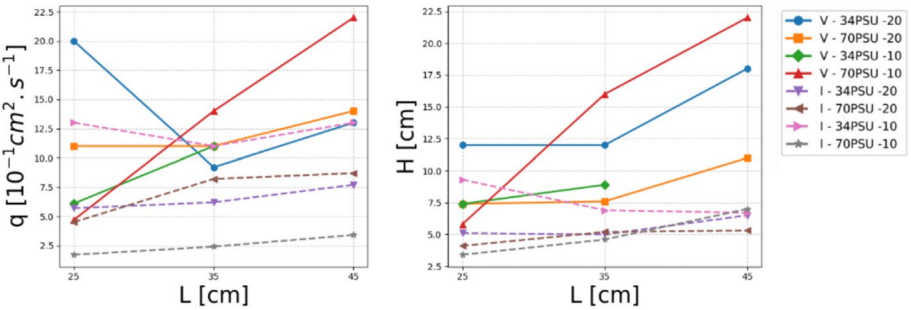

Fig. 7 Influence of the the opening size L on **q** and **H**. The vertical wall cases (V) are in solid lines and the inclined wall cases (I) are in dotted lines

difference between the lowest and the greatest values. This difference clearly shows that parameters have an influence on the values of q and H.

The parameter most consistently associated with an increase in both q and H was the opening size of the polynya as can be seen in Fig. 7. This result aligns with the intuition, as a larger opening size allows for increased ice formation and brine rejection. However, significant variability in the magnitude of this effect was observed. Under constant temperature, salinity, and geometric conditions, increasing the opening size from 25 to 45 cm can have an effect that ranges from multiplying the flow rate by 1.25 to multiplying it by 4.5.

The geometry of the lateral wall was also found to have a significant impact as can be seen in Fig. 7. The cases with a vertical wall exhibited higher values of both q and H compared to the same case with the other geometry. Similarly to the opening size effect, the range of the influence of the geometry varied considerably, ranging from negligible changes to a doubling of the flow rate. This variation is likely due to the increase in mixing and friction along the longer flow path when an inclined wall is present and the smaller effect of gravity due to the angle.

The role of water salinity was not as clear as that of the size of the polynya opening and the slope. As indicated by results reported in Table 3, the salt flux increases with salinity, suggesting that the flow rate q should also increase with higher salinity. In Table 2, this trend is observed for q in the majority of cases; however, exceptions occur for the opening size of 25 cm with the vertical wall and for half of the cases with the inclined wall. In general, the increase of q with salinity is quite small. Differently, for H, no significant trend was observed with respect to salinity.

The role of temperature in the experiments remains somewhat ambiguous. The expected outcome is that lower temperatures would lead to increased ice formation, resulting in greater brine rejection and, consequently, a higher flow rate. This expectation is supported by the data in Table 3, where a clear increase in salt flux is observed at lower temperatures. However, in Table 2, the values of q were not consistently higher in the lower temperature cases ($-$ 20 °C). In fact, in many instances, the opposite trend was observed. For H, no significant trend was observed with respect to temperature.

3.5 Discussion

As highlighted in Table 2, there are two clear trends that arise from our results: (i) the effect of the opening of the polynya and (ii) the effect of the slope. Both q and H increased with the increase of the opening and both q and H were greater in the case of the vertical wall than in the case of the slope, all other parameters being equal. The effect of the temperature and the salinity are instead not so clear. It would be expected that the decrease of the temperature and the increase in the salinity should give greater q. Table 3 clearly indicates that the salt flow induced by brine rejection followed this trend. Table 2 shows that in the case of the salinity, q seems to increase with the increase of salinity but not H. Conversely neither q nor H were found to follow a particular trend with respect to the temperature. This is surprising and remains unexplained. Further experiments will be needed to clarify this behavior.

Apart from understanding the role of the different parameters, the results of Table 3 also allow us to conduct a scaling analysis that can help explain the order of the average velocity measured in the experiments. Table 3 indicates a salt flux on the order of 10^{-2} g/m^2/s at $-$ 20 C for a salinity of the water of 34 PSU. For these conditions and an opening size of 35 cm, the average velocity was found to be on the order of magnitude of a few millimeters per second. Given that the surface area of the polynya is 0.245 m^2, during the 30-min duration of a single experiment, this flux results in the injection of approximately 4.4 g of salt. In a total volume of about 0.1 m^3, this leads to an increase in salinity of 0.044 PSU. With the haline contraction coefficient being β_S=0.78×10^{-3} PSU^{-1}, the corresponding relative increase in density is calculated as $\Delta\rho/\rho = \beta_S \Delta S = 3.4 \times 10^{-5}$.

From dimensional analysis, the velocity associated with buoyancy-induced natural convection can be expressed as $u \sim \sqrt{gl\Delta\rho/\rho}$, where l represents the length scale relevant to the flux. In this case, we can select l as the width of the boundary layer, 5 cm. This yields a final average velocity estimate of $u \sim 4$ mm/s, which is what was found in the experiments.

From these values, it is instructive to derive the pure numbers that control the experiments, namely the Prandtl, Reynolds, and Rayleigh numbers. The Prandtl number, Pr=ν/α, where ν is the kinematic viscosity and α is the thermal diffusivity, is equal to 14 for water at the freezing temperature. The Reynolds number reads $Re = uL/\nu$, where u is the typical velocity, L is the length scale, and ν is the kinematic viscosity. The experiments provide u around 0.3 cm/s and the characteristic length can be set equal to the opening of the polynya, namely $L = 35$ cm. This provides $Re \sim 1000$ which is compatible with a laminar flow, in agreement with measurements.

The Rayleigh number reads Ra=$gL^3\Delta\rho/(\mu\alpha)$, where μ is the dynamic viscosity, α is the thermal diffusivity and $\Delta\rho$ the density difference induced by the brine rejection. After adopting the order of magnitude analysis reported above, we find $\Delta\rho$=$\rho_0\beta_s\Delta S$=0.034 kg/m^3. This gives a large value of the Rayleigh number, around 5.5×10^7, indicating a prevalence of convection effects as observed in the experiments. In the case of a Rayleigh–Bénard cell, such a large value of the Rayleigh number usually implies a turbulent flow. However, this is not the case in our experiments, where we always observed clear laminar motions.

It is worth comparing the scales of different parameters and measurements from the experiments to their counterparts in the real polynyas. The opening length of a coastal polynya is typically 10 km, the depth of the ocean 3 km, and the inclination of the continental slope 1° to 3°. As for the formation of deep waters, the typical velocity along the slope is

0.5 m/s and the density difference between the dense water and the surrounding waters at the beginning of the slope is given mainly by the salinity difference which is 0.2 PSU, which gives a density difference of about 0.7 kg/m^3 [16]. These values imply very large values for both the Rayleigh and the Reynolds number far beyond their respective critical values.

To compare the experimental case to the field case, the Rayleigh number is much larger in the latter, but the qualitative meaning does not change, always indicating that convection dominates over diffusion. What changes substantially is the Reynolds number, which in the case of ocean polynyas is much larger than the critical one and indicates turbulent convective motions (differently from the approximately laminar motions observed in the experiments). This aspect suggests that—although qualitatively the results obtained here are to be considered valid also in real cases (i.e., the existence of currents totally induced by brine rejection)—caution is needed in transferring the quantitative aspects since turbulence could significantly alter them.

Indeed, some aspects that are not fully understood in the DSW and AABW formation are those regarding turbulent mixing [14]. Therefore, future experiments would have to face this issue. One possible solution would be to increase the brine rejection rate by increasing the heat exchange above the ice (e.g., by mean of forced convection).

4 Conclusion

Experiments on gravity currents using brine rejection as a source of buoyancy were carried out. The source of buoyancy resembled a polynya-like condition in a controlled laboratory environment. The experiments examined the effects of polynya size, external temperature, water salinity, and bottom geometry on the resulting velocity field.

The key result was to demonstrate that brine rejection is capable of generating clear gravity currents, having velocity (in our experimental setup) of the order magnitude of millimeters per second. Both the flow rate and the thickness of the current were found to vary depending on the experimental parameters. Specifically, increasing the polynya opening size led to higher flow rates and thicker currents. The flow rate was also slightly increased with the salinity of the water. In addition, the flow rate and current thickness were greater when a vertical wall was present, compared to configurations with a vertical wall. The wall inclination also influenced the structure of the motion due to the brine rejection: the vertical wall induced a cell structure resembling Rayleigh–Bénard flow, while more defined and developed currents were observed along the inclined wall. Finally, changes in external air temperature within the tested range did not significantly influence the flow rate or current thickness, though no clear physical mechanism was identified to explain this result.

Acknowledgements We wish to thank Andrea Cagninei and Roberto Bosio for their valuable help in the laboratory work.

Author contributions Nathan Cadot collected the experimental data, prepared the figures and wrote the article draft. Carlo Camporeale, Luca Ridolfi, and Pietro Salizzoni contributed equally to the conceptualization and supervision of the research, and the proofreading of the manuscript.

Funding Open access funding provided by École Centrale de Lyon. The project has been partially funded by the project climate_change@polito (Department of Excellence) by the Italian Ministry of University and research.

Data availability A Zenodo repository was created with the mean velocity field of the experiment extracted with the PIV software. https://doi.org/10.5281/zenodo.14925304

Code availability Not applicable

Declarations

Conflict of interest The authors declare that they have no known competing financial interests or personal relationships that have influenced the work reported in this paper.

Ethics approval and consent to participate Not applicable.

Consent for publication Not applicable.

References

1. Al-Achi A (2019) The student's t-test: a brief description. Res Rev J Hosp Clin Pharm 5(1):1
2. Allen S, Durrieu de Madron X (2009) A review of the role of submarine canyons in deep-ocean exchange with the shelf. Ocean Sci 5(4):607–620
3. Amblas D, Dowdeswell J (2018) Physiographic influences on dense shelf-water cascading down the antarctic continental slope. Earth Sci Rev 185:887–900
4. Baines PG, Condie S (1998) Observations and modelling of antarctic downslope flows: A review. Ocean Ice Atmos Interact Antarct Cont Margin Antarct Res Ser 75:29–49
5. Britter R, Linden P (1980) The motion of the front of a gravity current travelling down an incline. J Fluid Mech 99(3):531–543
6. Brown WS (2016) Physical properties of seawater. Springer, Berlin, pp 101–110
7. Ebner L, Heinemann G, Haid V et al (2014) Katabatic winds and polynya dynamics at coats land, Antarctica. Antarct Sci 26(3):309–326
8. Foster TD (1969) Experiments on Haline convection induced by the freezing of sea water. J Geophys Res 74(28):6967–6974
9. Foster TD, Carmack EC (1976) Frontal zone mixing and Antarctic bottom water formation in the southern Weddell sea. Deep sea research and oceanographic abstracts. Elsevier, Amsterdam, pp 301–317
10. Kämpf J (2005) Cascading-driven upwelling in submarine canyons at high latitudes. J Geophys Res Oceans. https://doi.org/10.1029/2004JC002554
11. Lake R, Lewis E (1970) Salt rejection by sea ice during growth. J Geophys Res 75(3):583–597
12. Manabe S, Stouffer RJ (1999) The role of thermohaline circulation in climate. Tellus B 51(1):91–109
13. Mensah V, Nakayama Y, Fujii M et al (2021) Dense water downslope flow and AABW production in a numerical model: Sensitivity to horizontal and vertical resolution in the region off cape darnley polynya. Ocean Model 165:101843
14. Miller UK, Zappa CJ, Gordon AL et al (2024) The coupling of winds, ocean turbulence, and high salinity shelf water in the terra nova bay polynya. Deep Sea Res Part II 218:105412
15. Moore D, Weiss N (1973) Two-dimensional Rayleigh-bénard convection. J Fluid Mech 58(2):289–312

16. Muench RD, Gordon AL (1995) Circulation and transport of water along the western Weddell sea margin. J Geophys Res Oceans 100(C9):18503–18515
17. Mustafa J, Ghasem N, El-Naas MH et al (2024) Cfd modeling for optimal electrodialysis: valorizing reject brine and carbon dioxide for sustainable solutions. Sep Purif Technol 328:125083
18. Negretti ME, Flor JB, Hopfinger EJ (2017) Development of gravity currents on rapidly changing slopes. J Fluid Mech 833:70–97
19. Negretti ME, Tucciarone FL, Wirth A (2021) Intruding gravity currents and re-circulation in a rotating frame: laboratory experiments. Phys Fluids 33(9):096607
20. Niedrauer TM, Martin S (1979) An experimental study of brine drainage and convection in young sea ice. J Geophys Res Oceans 84(C3):1176–1186
21. O'hern T, Weckman E, Gerhart A et al (2005) Experimental study of a turbulent buoyant helium plume. J Fluid Mech 544:143–171
22. Ohshima KI, Fukamachi Y, Williams GD et al (2013) Antarctic bottom water production by intense sea-ice formation in the cape Darnley polynya. Nat Geosci 6(3):235–240
23. Shapiro G, Huthnance J, Ivanov V (2003) Dense water cascading off the continental shelf. J Geophys Res Oceans. https://doi.org/10.1029/2002JC001610
24. Silvano A, Purkey S, Gordon AL et al (2023) Observing Antarctic bottom water in the southern ocean. Front Mar Sci 10:1221701
25. Talley LD (2002) Salinity patterns in the ocean. Earth Syst Phys Chem Dimens Global Environ Change 1:629–640
26. Tamura T, Ohshima KI, Nihashi S (2008) Mapping of sea ice production for Antarctic coastal polynyas. Geophys Res Lett. https://doi.org/10.1029/2007GL032903
27. Thielicke W, Sonntag R (2021) Particle image velocimetry for MATLAB: accuracy and enhanced algorithms in PIVlab. J Open Res Soft 9(1):12
28. Ushio S, Wakatsuchi M (1993) A laboratory study on supercooling and frazil ice production processes in winter coastal polynyas. J Geophys Res Oceans 98(C11):20321–20328
29. Wells M, Wettlaufer J (2005) Two-dimensional density currents in a confined basin. Geophys Astrophys Fluid Dyn 99(3):199–218
30. Worster G, Moffatt K, Batchelor G (2000) Perspectives in fluid dynamics: a collective introduction to current research. Cambridge University Press, Cambridge
31. Zheng W, Zhaoru Z, Vihma T et al (2021) An overview of Antarctic polynyas: sea ice production, forcing mechanisms, temporal variability and water mass formation. Adv Polar Sci 32(4):295–311